Hubbard-*U* calculations for Cu from first-principle Wannier functions

I. Schnell and G. Czycholl
Department of Physics, University of Bremen, P.O. Box 330 440, D-28834 Bremen, Germany

R. C. Albers
Theoretical Division, Los Alamos National Laboratory, Los Alamos, New Mexico 87545

(Received 16 May 2001; revised manuscript received 17 September 2001; published 18 January 2002)

We present first-principles calculations of optimally localized Wannier functions for Cu and use these for an *ab initio* determination of Hubbard (Coulomb) matrix elements. We use a standard linearized muffin-tin orbital calculation in the atomic-sphere approximation to calculate Bloch functions, and from these determine maximally localized Wannier functions using a method proposed by Marzari and Vanderbilt. The resulting functions were highly localized, with greater than 89% of the norm of the function within the central site for the occupied Wannier states. Two methods for calculating Coulomb matrix elements from Wannier functions are presented and applied to fcc Cu. For the unscreened on-site Hubbard *U* for the Cu 3d bands, we have obtained about 25 eV. These results are also compared with results obtained from a constrained local-density approximation calculation.

DOI: 10.1103/PhysRevB.65.075103 PACS number(s): 71.10.Fd, 71.15.Ap, 71.27.+a

I. INTRODUCTION

During the past few decades powerful numerical methods have been developed for the *ab initio* (first-principles) calculation of the electronic ground-state properties of solids. In most of these methods density-functional theory[1] (DFT) has been used to treat the electron-electron Coulomb repulsion, and a local-density approximation[2] (LDA) (or a local spin-density approximation for magnetic systems) has been used for the exchange-correlation potential. This procedure has been very successful for many materials and ground-state properties (e.g., crystal structure, lattice constant, binding energy, and ionization energy), but it has its limitations; the band gap of semiconductors is not properly reproduced, for instance. Furthermore, for systems such as high-temperature superconductors, heavy-fermion materials, transition-metal oxides, and 3d itinerant magnets, i.e., for systems in which the Fermi level falls into a region of narrow energy bands, the LDA is usually not sufficient. It is generally accepted that the problem for these materials is the strong electronic correlations that are responsible for their electronic properties. For a description of such strongly correlated systems, one usually instead uses as a starting point model Hamiltonians like the Hubbard model[3] and its multiband generalizations. But in these models the Coulomb (interaction) matrix elements and also the one-particle (hopping) matrix elements that determine the unperturbed band structure are usually treated as free, adjustable parameters, i.e., they are not known from ''first principles'' for the given material; on the other hand, Coulomb correlations can be studied within reliable many-body approximations that go beyond the Hartree-Fock approximation.

Both the *ab initio* LDA and the many-body model-Hamiltonian methods based on Hubbard-like models have their merits, but until rather recently they have been almost separate and complementary approaches. But, in view of the power of each, a combination of these methods is desirable; and, in fact, during the last few years there have been some attempts in this direction.[4–14] All of these recent developments add local, screened Coulomb (Hubbard) correlations U between localized orbitals to the one-particle part of the Hamiltonian obtained from an *ab initio* LDA band-structure calculation, but differ in how they handle the correlation part. In the earliest attempts, the LDA+U method[4] used essentially a static mean-field-like (or Hubbard-I-like) approximation for the correlation. The simplest approximation beyond the Hartree-Fock approximation, second-order perturbation theory in U, was used[5,6,9,13] to study the electronic properties of 3d systems (like Fe and Ni) and heavy-fermion systems (like UPt_3). The LDA++ approach[8,10,11] has a similar strategy, but uses other many-body approximations to treat the correlation problem, namely, either the fluctuation-exchange approximation or the dynamical mean-field theory[15] (DMFT). Some of the other many-body treatments[7,12,14] have also used DMFT, which is based on the limit of large-dimension ($d\rightarrow\infty$) approximation for correlated lattice electrons.[16] Within DMFT the self-energy becomes local, i.e., independent of momentum *k*, which allows a mapping of the lattice problem onto an effective impurity model. The LDA+DMFT treatments[10–14] mentioned above differ in the many-body method they used for the effective impurity problem, namely, quantum Monte Carlo,[14] the noncrossing approximation,[12] or iterated perturbation theory.[7] But all these approaches, including the LDA+U, have in common that they have to introduce a Hubbard U as an additional parameter, and hence are not real first-principles (*ab initio*) treatments. Although they use an LDA *ab initio* method to obtain a realistic band structure, i.e., single-particle properties, Coulomb matrix elements for any particular material are not known, and the Hubbard U remains an adjustable parameter.

One can obtain estimates on the magnitude of *U* either from experiment (high-energy spectroscopy) or from the constrained LDA method.[4,17–22] Within the latter method one adds the constraint that the electron occupation number for the correlated bands is fixed to a given number through a

Lagrange parameter. One can then use LDA to calculate the ground-state energy for different occupations of the correlated states, and the difference between the energy for double and single occupation is an estimate for the Hubbard U. This method has the advantage that effects of screening are already somehow included. On the other hand there are usually several bands and many interaction matrix elements (on-site, density-density, intraband, interband, exchange, intersite, etc.) that have different magnitudes, and the constrained LDA can only give some average value for these various Coulomb matrix elements and not the individual *ab initio* parameters (Coulomb matrix elements). This approach is intuitive and contains some type of screening within a one-electron LDA approach. It is difficult to sort out the actual approximation involved.

In this paper we suggest a different approach, namely, the direct *ab initio* calculation of the one-particle (tight-binding) and two-particle (Coulomb) matrix elements. Our starting point is a standard electronic band-structure calculation, for which we have used the linearized muffin-tin orbital (LMTO) method[23,24] within the atomic-sphere approximation (ASA). The LDA band-structure calculation yields not only one-particle energies but also their eigenstates, the Bloch wave functions, which form a proper basis of a one-particle Hilbert space. To determine the local (onsite and intersite) Coulomb matrix elements it is necessary to construct Wannier functions,[25,26] which are closely related to the Bloch functions via a unitary transformation, but which are not unique since the phases of the Bloch functions are undetermined.

As first suggested by Marzari and Vanderbilt,[27] this gauge freedom can be used to construct ''maximally localized Wannier functions.'' Those are just Wannier functions with a special gauge that makes them optimally localized according to some criterion. A proper localization of the Wannier functions is important in our opinion, because only then do the standard assumptions of the model treatments hold such that only a few (on-site, nearest, and next-nearest neighbor) one-particle (hopping) and two-particle (Coulomb) matrix elements have to be considered explicitely. These matrix elements can then be calculated from the Wannier functions.

We use two different methods to calculate Coulomb matrix elements from Wannier functions. The first method uses the fact that the LMTO method provides Bloch functions in the basis of linear muffin-tin orbitals.[23] Therefore the Wannier functions are given as linear combinations of such muffin-tin orbitals as well, and can be used to evaluate the Coulomb integrals efficiently, similarly to what was done in Ref. 28. The second method uses a fast Fourier transformation (FFT). It does not rely on the property of the wave functions being linear and is therefore more general. It is also very quick and efficient.

The paper is organized as follows. In Sec. II we present some of the computational details: we describe the form of the Bloch functions in the LMTO method, how to obtain the Wannier functions from them, and how to optimize the choice of the Wannier functions by using the Marzari-Vanderbilt method. Then we describe how the one-particle (hopping) matrix elements are obtained from these localized Wannier functions, and we present the two methods to calculate the Coulomb matrix elements. To illustrate the method, we have performed actual calculations for a well-understood system, namely, for Cu. Although this material is not a strongly correlated system, it has almost completely filled, narrow 3d bands, for which (well-localized) Wannier functions and one- and two-particle matrix elements can be calculated. Results for Cu are presented in Sec. III, where we show some of the Wannier functions, demonstrate how well localized they are and that the one-particle (tight-binding) matrix elements obtained from them allow for a reconstruction of the band structure. The direct Coulomb matrix elements obtained are rather large, between 20 and 25 eV for Wannier states with mainly 3d character, and are about 5 eV for nearest neighbors and about 1 eV for exchange interactions. In Sec. IV we describe constrained LDA calculations, which yield somewhat smaller values (about 18 eV) for the Hubbard U of Cu, and in the final section (V) we discuss how to extend and further apply the current approach.

II. COMPUTATIONAL DETAILS

We restrict ourselves to the case where there is only one atom per unit cell and where we can neglect spin (non-spin-polarized calculations). For a given material the only input to an *ab initio* LDA calculation is the atomic number. In the density-functional approach,[1,29] a local-density approximation is normally used for the exchange and correlation interactions between the electrons; we have used the von Barth–Hedin[30] exchange-correlation potential and a frozen-core approximation. Within DFT the total energy of the ground state could be calculated as a function of volume for a given crystal structure and used to determine the equilibrium lattice constant; it is usually in good agreement with experiment. However, since our focus is on the determination of Coulomb matrix elements in a Wannier basis, we have simply used the experimental lattice parameters.

A. LMTO wave functions

For our band-structure results we have used the LMTO method[23,24] within the ASA. The combined correction term[23] was not included. The muffin-tin spheres are overlapping and their radius (the Wigner-Seitz radius S) is determined by the condition that the sphere volume equals the volume of the unit cell. Within the muffin-tin spheres the potential and wave functions are expanded in spherical harmonics with a cutoff $l_{\max}=3$, i.e., s, p, d, and f orbitals are included. Furthermore, the Bloch wave functions are given in terms of the solution to the radial Schrödinger equation $\phi_{\nu l}(r)$ to some fixed energies $E_{\nu l}$ and its energy derivative $\dot{\phi}_{\nu l}(r)$,

$$\Psi_{n\mathbf{k}}(\mathbf{r})=\sum_{L}\left(\phi_{\nu l}(r)A_{L}^{n\mathbf{k}}+\dot{\phi}_{\nu l}(r)B_{L}^{n\mathbf{k}}\right)Y_{L}(\hat{\mathbf{r}}), \qquad (1)$$

where we use complex spherical harmonics in all of our calculations. This expansion is valid in one muffin-tin sphere. Here, as usual, $L=\{l,m\}$ is understood and n is the band index and $\mathbf{k}$ is the wave vector. We define n by the condition that $E_{n}(\mathbf{k})<E_{n+1}(\mathbf{k})$. The virtue of using this method for

Wannier functions is the simplification that only integrals over spheres are needed; no real-space integrations over complicated Wigner-Seitz (unit) cells are required.

The Bloch functions obey

$$\Psi_{n\mathbf{k}}(\mathbf{r}+\mathbf{R}) = e^{i\mathbf{k}\cdot\mathbf{R}}\Psi_{n\mathbf{k}}(\mathbf{r}). \tag{2}$$

Therefore, the knowledge of a Bloch function in a single muffin-tin sphere is sufficient for the knowledge of the function in the whole crystal. This situation is different when we consider Wannier functions, which can be centered on different sites. It is useful to introduce a notation that holds for both Bloch and Wannier functions. To do this we perform an expansion like Eq. (1) in each muffin-tin sphere, which we label by its site vector **R**. The complete wave function (either Bloch or Wannier) is then given by

$$\Phi_\alpha(\mathbf{r}) = \sum_i \Phi_\alpha(\mathbf{R}_i;\mathbf{r}-\mathbf{R}_i). \tag{3}$$

In this equation we have used the general notation for the wave-function expansion $\Phi_\alpha(\mathbf{R}_i;\mathbf{r}-\mathbf{R}_i)$. (i) Φ is any kind of wave function. (ii) α stands for quantum numbers (Bloch, $\alpha=\{n,\mathbf{k}\}$; Wannier, $\alpha=\{\mathbf{R},n\}$). (iii) The first argument in the parenthesis indicates the muffin-tin sphere about which we are expanding and is labeled by its site vector. (iv) The second argument in the parenthesis is the position inside this muffin-tin sphere described by its relative vector. This means that this vector has zero length in the center of the muffin-tin sphere described by the first argument. (v) Note that, for every **R**,

$$\Phi_\alpha(\mathbf{R};\mathbf{r}) = 0 \quad \text{if } |\mathbf{r}| > S. \tag{4}$$

In the case where Φ is a Bloch function we find

$$\Psi_{n\mathbf{k}}(\mathbf{R};\mathbf{r}) = e^{i\mathbf{k}\cdot\mathbf{R}}\Psi_{n\mathbf{k}}(\mathbf{r}). \tag{5}$$

It is easy to see that Eq. (5) inserted in Eq. (3) obeys Eq. (2).

Also note that Eq. (3) disregards the effects of overlapping muffin-tin spheres. Within the ASA approximation, all derivations are done as though nonoverlapping muffin tins are being used, and then these formulas are used with expanded muffin tins, whose volumes sum up to equal the unit cell-volume (where the muffin-tin radius is expanded to a Wigner-Seitz radius for one atom per unit cell). In addition, this approximation eliminates the necessity to handle interstitial regions, and hence the ASA formalism is mathematically much simpler than a full-potential electronic-structure calculation would require.

B. Wannier functions

In this section we show how to calculate Wannier functions from the LMTO type of Bloch functions of Eq. (1). The Wannier functions[25] are defined by

$$w_{\mathbf{R}n}(\mathbf{r}) \equiv \langle \mathbf{r}|\mathbf{R}n\rangle = \frac{1}{N}\sum_{\mathbf{k}} e^{-i\mathbf{k}\cdot\mathbf{R}}\Psi_{n\mathbf{k}}(\mathbf{r}). \tag{6}$$

Here, N is the number of **k**-mesh points in the Brillouin zone or, equivalently, the number of unit cells in the real-space supercell that is used to discretize the **k** mesh. As mentioned above, Wannier functions are not unique. Consider, for example, a single band n with Bloch functions $|\Psi_{n\mathbf{k}}\rangle$; a transformation of the kind

$$|\Psi_{n\mathbf{k}}\rangle \rightarrow e^{i\phi_n^{(\mathbf{k})}}|\Psi_{n\mathbf{k}}\rangle, \quad \text{for } \phi_n^{(\mathbf{k})} \text{ real} \tag{7}$$

will still lead to Bloch functions. We shall call this a gauge transformation of the first kind. In the case of a composite set of bands,[27] this nonuniqueness corresponds to the freedom to choose the phases and ''band-index labeling'' at each **k** point of the Bloch functions,

$$|\Psi_{n\mathbf{k}}\rangle \rightarrow \sum_m U_{mn}^{(\mathbf{k})}|\Psi_{m\mathbf{k}}\rangle. \tag{8}$$

We shall call this a gauge transformation of the second kind. Here $U_{mn}^{(\mathbf{k})}$ is a unitary matrix. From all the arbitrary choices of Wannier functions we will pick out that particular set that minimizes the total spread given by

$$\Omega = \sum_n [\langle r^2\rangle_n - \langle r\rangle_n^2]. \tag{9}$$

For any operator A, $\langle A\rangle_n$ denotes the expectation value $\langle \mathbf{R}n|A|\mathbf{R}n\rangle$. A method for minimizing Eq. (9) has been developed by Marzari and Vanderbilt[27] and its application to the ASA wave functions does not pose any particular problems (details will be given below).

Before minimizing Ω according to this procedure, it is useful to prepare the Bloch orbitals to make the starting Wannier functions somewhat localized. This has two advantages: (i) the minimization procedure converges faster and (ii) this helps to avoid getting trapped in local minima. Marzari and Vanderbilt[27] suggest several possible preparations. We have found our own method, which seems to work well. This involves a simple gauge transformation for each band, which is given by

$$\Psi_{n\mathbf{k}}(\mathbf{r}) \rightarrow \exp[-i\ \mathrm{Im}\ln\Psi_{n\mathbf{k}}(\mathbf{r}_0)]\Psi_{n\mathbf{k}}(\mathbf{r}). \tag{10}$$

This gauge transformation has the property that $\mathrm{Im}\ln\Psi_{n\mathbf{k}}(\mathbf{r}_0)$ transforms to zero. So at the point $\mathbf{r}_0$ all the Bloch functions will have the same phase (in this case just $1+i0$) and $\langle \mathbf{r}_0|\mathbf{0}n\rangle$ will take a large value. We thus expect the Wannier function to be fairly localized at $\mathbf{r}_0$. To make the method work well one should choose $\mathbf{r}_0$ where the Wannier functions are expected to be reasonably large. In our calculations we have chosen the direction of this vector to be well away from the expected zeros of the spherical harmonics and with an absolute value far enough away from the origin to be in a place where the Wannier functions should have a significant magnitude. We found an $\mathbf{r}_0$ of $(0.8, 1.0, 0.3)a_0$ to work well for fcc Cu.

We shall now derive expressions of the form of Eq. (3) for Wannier functions. From Eqs. (5) and (6) we have

$$w_{\mathbf{R}n}(\mathbf{R}';\mathbf{r}) = \frac{1}{N}\sum_{\mathbf{k}} e^{-i\mathbf{k}\cdot\mathbf{R}}\Psi_{n\mathbf{k}}(\mathbf{R}';\mathbf{r})$$

$$= \frac{1}{N}\sum_{\mathbf{k}} e^{i\mathbf{k}\cdot(\mathbf{R}'-\mathbf{R})}\Psi_{n\mathbf{k}}(\mathbf{r}). \quad (11)$$

Because Wannier functions on different sites have the same form (shape) of their wave functions and differ only by a translation of their origin, it is useful to use a notation that indicates values of a wave function relative to a Wannier function centered at the origin,

$$w_{\mathbf{R}n}(\mathbf{R}';\mathbf{r}) = w_{\mathbf{0}n}(\mathbf{R}'-\mathbf{R};\mathbf{r}) \equiv w_n(\mathbf{R}'-\mathbf{R};\mathbf{r}), \quad (12)$$

where we have introduced the notation $w_{\mathbf{0}n} \equiv w_n$ (i.e., if the subscript contains only a wave function label without a spatial vector $\mathbf{R}$, then we are using a relative notation that refers to a Wannier function centered at the origin). We can use the Bloch condition [cf. Eq. (11)] to calculate the parts of the Wannier function on other sites $\mathbf{R}$,

$$w_n(\mathbf{R};\mathbf{r}) = \frac{1}{N}\sum_{\mathbf{k}} e^{i\mathbf{k}\cdot\mathbf{R}}\Psi_{n\mathbf{k}}(\mathbf{r}). \quad (13)$$

Note that $|\mathbf{r}| < S$. For this notation to work in our numerical calculations, it is essential to force the Wannier center, i.e., the muffin-tin sphere where $\langle \mathbf{r}|\mathbf{0}n\rangle$ is largest, to be at the muffin-tin sphere around the lattice site $\mathbf{0}$; we achieve this by setting $|\mathbf{r}_0| < S$ in Eq. (10). In most of the rest of the paper, we will almost always use the relative notation that refers to Wannier states centered at the origin, and will perform whatever translations are necessary to be able to use these states.

In the method of Marzari and Vanderbilt,[27] the starting point for the calculations are a set of reference matrices defined by

$$M_{mn}^{(0)(\mathbf{k},\mathbf{b})} = \langle \Psi_{m\mathbf{k}}|e^{-i\mathbf{b}\cdot\mathbf{r}}|\Psi_{n,\mathbf{k}+\mathbf{b}}\rangle. \quad (14)$$

Here $\mathbf{b}$ denotes a nearest-neighbor vector on the discretized mesh in $\mathbf{k}$ space (in this method, the set of $\mathbf{b}$ vectors are needed for numerical derivatives). We calculated the action of $e^{-i\mathbf{b}\cdot\mathbf{r}}$ on the ket by using Eqs. (A4) and (A2) and solved the remaining integral by using Eq. (22). We used a uniform (cubic) discrete $\mathbf{k}$ mesh with a spacing Δk of $0.2(2\pi/a)$. In such a mesh there are six nearest neighbors for the $\mathbf{b}$ vectors needed for the numerical derivatives. We were careful not to double count vectors in the $\mathbf{k}$ mesh (those equivalent to each other by a reciprocal lattice vector) within the Brillouin zone (BZ) (which has 500 $\mathbf{k}$ points in the full zone).

We then used the steepest-descent method and relevant equations in Sec. IV of Ref. 27 to iterate a series of small steps where a set of $\Delta W^{\mathbf{k}}$ were calculated and used to update the unitary matrices $U^{\mathbf{k}}$ and the $M^{\mathbf{k},\mathbf{b}}$ matrices. After each iteration, where we update all the relevant $\mathbf{k}$ matrices, we calculated the spread function Ω, and continued iterating until this converged.

In these calculations the initial matrices $M^{(0)(\mathbf{k},\mathbf{b})}$ are by far the most time consuming computationally (it requires storing $6\times500\times16^2 = 768\,000$ complex numbers). The iterations of the steepest-descent method were much faster. For this reason we used many iterations (about 1500 steps) and converged Ω to about 0.01%. For the step size [cf. Eq. (57) of Ref. 27] we used an α of 0.2.

The final result can be written in a form similar to the LMTO wave functions, Eq. (1),

$$w_n(\mathbf{R};\mathbf{r}) = \sum_L (\phi_{\nu l}(r)A_L^{n\mathbf{R}} + \dot{\phi}_{\nu l}(r)B_L^{n\mathbf{R}})Y_L(\hat{\mathbf{r}}), \quad (15)$$

where the A and B matrices originally come from the LMTO wave functions, but are then updated from the relevant phase information, unitary matrix, and other integrations and transformations of the method.

Because of the normalization of the starting LMTO Bloch wave functions (which are normalized to unity within a single unit cell), each Wannier function is naturally normalized to unity when integrated over all space.

C. One-particle matrix elements

The Wannier function basis can be viewed as an orthogonal tight-binding basis. For this reason it is useful to calculate one-particle matrix elements of the Hamiltonian in the Wannier basis. As we shall see, these matrix elements are (for a gauge transformation of the first kind only) equivalent to the Fourier components of the band structure; this equivalence is useful for checking some of the numerical aspects of the calculations.

Because the Hamiltonian has the property that $H(\mathbf{r}) = H(\mathbf{r}+\mathbf{R})$, it is sufficient to consider the matrix elements

$$t_{\mathbf{R}nm} \equiv \langle \mathbf{R}n|H|\mathbf{0}m\rangle. \quad (16)$$

Inserting Eq. (6) and using $H|\Psi_{n\mathbf{k}}\rangle = E_n(\mathbf{k})|\Psi_{n\mathbf{k}}\rangle$ we find

$$t_{\mathbf{R}nm} = \frac{\delta_{nm}}{N}\sum_{\mathbf{k}} e^{i\mathbf{k}\cdot\mathbf{R}}E_n(\mathbf{k}), \quad (17)$$

which are just the Fourier components of the band structure. The Bloch states $|\Psi_{n\mathbf{k}}\rangle$ continue to be eigenstates of H under a gauge transformation of the first kind and one can also easily show that the $t_{\mathbf{R}nm}$ are invariant under this type of gauge transformation. The $t_{\mathbf{R}nm}$ from Eq. (17) can be directly calculated from the band structure $E_n(\mathbf{k})$.

A gauge transformation of the second kind leads to states $|\Psi_{n\mathbf{k}}\rangle$ that are no longer eigenstates of H with eigenvalue $E_n(\mathbf{k})$. Therefore $t_{\mathbf{R}nm}$ are not invariant under a gauge transformation of the second kind. However, generally we can always calculate

$$H_{nm}^{\mathbf{k}} \equiv \langle \Psi_{n\mathbf{k}}|H|\Psi_{m\mathbf{k}}\rangle = \sum_{\mathbf{R}} e^{-i\mathbf{k}\cdot\mathbf{R}}t_{\mathbf{R}nm} \quad (18)$$

and use its diagonalized eigenvalues as the band structure for any set of Wannier functions. The matrix $H_{nm}^{\mathbf{k}}$ is Hermitian; it is, of course, already diagonal for a gauge transformation of the first kind, with the energy levels as the diagonal matrix elements.

To calculate $t_{\mathbf{R}nm}$ from Eq. (16), i.e., using Wannier functions, we can use Eqs. (3) and (12) to find

$$t_{\mathbf{R}nm}=\sum_i \int d^3\mathbf{r}\, w_n^*(\mathbf{R}_i-\mathbf{R};\mathbf{r})Hw_m(\mathbf{R}_i;\mathbf{r}), \tag{19}$$

where the integral is over a single sphere only. The effect of H on the second wave function can be carried out easily because we are working in a linear basis. We only note that $(H-E_{\nu l})\phi_l(r)=0$ and $(H-E_{\nu l})\dot{\phi}_l(r)=\phi_l(r)$, for details see Ref. 23. In order to calculate Eq. (19), we must evaluate integrals of the form

$$I=\int d^3\mathbf{r}\, f_1^*(\mathbf{r})f_2(\mathbf{r}), \tag{20}$$

where the functions $f_i(\mathbf{r})$ are given by the expansion

$$f_i(\mathbf{r})=\sum_L R_{iL}(r)Y_L(\hat{\mathbf{r}}). \tag{21}$$

Inserting Eq. (21) into Eq. (20) and using the orthonormality of the spherical harmonics yields

$$I=\sum_L \int dr\, r^2\ R_{1L}^*(r)R_{2L}(r). \tag{22}$$

Because Eq. (1) was our starting point, the radial functions $R(r)$ will always be given in terms of $\phi_l(r)$ and $\dot{\phi}_l(r)$, i.e.,

$$R_{iL}(r)=A_{iL}\phi_l(r)+B_{iL}\dot{\phi}_l(r). \tag{23}$$

We will use this form to calculate the integral I very efficiently. It is clear that any integral can be reduced to a linear combination of ''basic'' integrals. Those basic integrals consist of the (very limited) combinations of the $\phi_l(r)$'s and $\dot{\phi}_l(r)$'s. We will label them by

$$b_{l;p_1p_2}=\int dr\, r^2[\delta_{p_1,0}\phi_l(r)+\delta_{p_1,1}\dot{\phi}_l(r)] \times[\delta_{p_2,0}\phi_l(r)+\delta_{p_2,1}\dot{\phi}_l(r)], \tag{24}$$

where p_1 and p_2 can take the values 0 and 1. So it must be possible to write the integral I as

$$I=\sum_L \sum_{p_1=0}^{1}\sum_{p_2=0}^{1} a_{L;p_1p_2}b_{l;p_1p_2}. \tag{25}$$

It follows that the coefficients $a_{L;p_1p_2}$ are given by

$$a_{L;p_1p_2}=[\delta_{p_1,0}A_{1L}^*+\delta_{p_1,1}B_{1L}^*][\delta_{p_2,0}A_{2L}+\delta_{p_2,1}B_{2L}]. \tag{26}$$

We are now in a position to calculate Eq. (19) with the aid of Eq. (25).

D. Wannier-function projected density of states

The density of states (DOS) per spin is defined by

$$N(E)=\frac{V}{(2\pi)^3}\sum_n \int_{\mathrm{BZ}} d^3\mathbf{k}\,\delta(E-E_n(\mathbf{k})), \tag{27}$$

where V is the volume of the unit cell. In the same way that the DOS is often projected in terms of the l character of the states, one can do a similar treatment for a projection onto the Wannier states. We can define a projected DOS for Wannier states, by inserting the projection operator onto the Wannier states $|\mathbf{0}j\rangle\langle\mathbf{0}j|$ into Eq. (27),

$$N_j(E)=\frac{V}{(2\pi)^3}\sum_n \int_{\mathrm{BZ}} d^3\mathbf{k}|\langle\psi_{n\mathbf{k}}|\mathbf{0}j\rangle|^2\delta(E-E_n(\mathbf{k})). \tag{28}$$

Note that the $\psi_{n\mathbf{k}}$ in this formula have to be the Bloch states before the gauge transformation, since the band structure $E_n(\mathbf{k})$ is related to the untransformed states. The Bloch wave functions are normalized to a single unit cell and each Wannier function over all space. We can calculate $N_j(E)$ by using the tetrahedron method.[31] For the $\mathbf{k}$ points that form the tetrahedrons we need to calculate $|\langle\psi_{n\mathbf{k}}|\mathbf{0}j\rangle|^2$, which we have done using the scheme described in Sec. II C. In these calculations it is important to be aware that $|\mathbf{0}j\rangle$ has parts of its wave function on sites other than the central site where it is centered. In our calculations, we included parts of the Wannier function out to 17 near-neighbor shells of sites.

Note that the exact projection operator is a sum over all $\mathbf{R}$, since

$$\sum_{\mathbf{R}j}|\mathbf{R}j\rangle\langle\mathbf{R}j|=1. \tag{29}$$

However, it is sufficient to only consider the Wannier states $|\mathbf{0}j\rangle$ in our projection (and not all the $|\mathbf{R}j\rangle$), since

$$|\langle\psi_{n\mathbf{k}}|\mathbf{R}j\rangle|=|\langle\psi_{n\mathbf{k}}|\mathbf{0}j\rangle|. \tag{30}$$

We can check the correctness of our projection by comparing $N_{\mathrm{tot}}(E)=\Sigma_j N_j(E)$ with the $N(E)$ that is calculated directly from the LMTO energy eigenvalues. We find that our projected sum is accurate to within 0.2% of the LMTO value.

E. Coulomb matrix elements

The matrix elements we wish to calculate are

$$W_{12,34}=\int \frac{d^3\mathbf{r}\,d^3\mathbf{r}'e^2}{|\mathbf{r}-\mathbf{r}'|}w_1^*(\mathbf{r})w_2^*(\mathbf{r}')w_3(\mathbf{r})w_4(\mathbf{r}'). \tag{31}$$

where $1,2,3,4=i=\{\mathbf{R}_i n_i\}$ is a Wannier state and W denotes the Coulomb interaction. The spatial integrals over $\mathbf{r}$ and $\mathbf{r}'$ extend over all space. Using Eqs. (3) and (12), we can use translations to rewrite this expression so that the integrals are only over the muffin-tin sphere at the origin,

$$W_{12,34}=\sum_{i,j} W(12,34;\mathbf{R}_i,\mathbf{R}_j), \tag{32}$$

where the expression $W(12,34;\mathbf{R},\mathbf{R}')$ is defined by

$$\int \frac{d^3\mathbf{r}\,d^3\mathbf{r}'e^2}{|\mathbf{r}-\mathbf{r}'+\mathbf{R}-\mathbf{R}'|} w^*_{n_1}(\mathbf{R}-\mathbf{R}_1;\mathbf{r}) w^*_{n_2}(\mathbf{R}'-\mathbf{R}_2;\mathbf{r}') \times w_{n_3}(\mathbf{R}-\mathbf{R}_3;\mathbf{r}) w_{n_4}(\mathbf{R}'-\mathbf{R}_4;\mathbf{r}'). \quad (33)$$

Since most applications of the Hubbard model use only two orbitals instead of all four, it is useful to define the limiting subset of the W functions as direct Coulomb U_{ij} and exchange J_{ij} integrals,

$$U_{12}=W_{12,12}, \quad J_{12}=W_{12,21} \quad (34)$$

and the obvious generalizations for

$$U(12;\mathbf{R},\mathbf{R}')=W(12,12;\mathbf{R},\mathbf{R}'),$$

$$J(12;\mathbf{R},\mathbf{R}')=W(12,21;\mathbf{R},\mathbf{R}'). \quad (35)$$

1. Spherical-harmonics expansion

We will now only consider matrix elements between Wannier functions centered on the origin [i.e., where the $\mathbf{R}_i=\mathbf{0}$ in Eq. (31)]. Because we are using maximally localized Wannier functions, most of the Wannier functions have their largest component in the center cell (see Sec. III). As a first approximation, we will therefore neglect all other muffin-tin spheres. This approximation allows us to calculate on-site interband matrix elements. We are thus looking for

$$W_{n_1n_2,n_3n_4}\approx W(12,34;\mathbf{0},\mathbf{0})=\int d^3\mathbf{r}\,d^3\mathbf{r}' w^*_{n_1}(\mathbf{0};\mathbf{r}) w^*_{n_2}(\mathbf{0};\mathbf{r}') \times \frac{e^2}{|\mathbf{r}-\mathbf{r}'|} w_{n_3}(\mathbf{0};\mathbf{r}) w_{n_4}(\mathbf{0};\mathbf{r}'), \quad (36)$$

where the integral over $\mathbf{r}$ is only over the central site. Inserting the expansion Eq. (21) for the Wannier functions and making use of the well-known expansion (see, for example, Ref. 32)

$$\frac{1}{|\mathbf{r}-\mathbf{r}'|}=\sum_{l=0}^{\infty}\frac{4\pi}{2l+1}\frac{r_<^l}{r_>^{l+1}}\sum_{m=-l}^{l} Y^*_L(\hat{\mathbf{r}}')Y_L(\hat{\mathbf{r}}), \quad (37)$$

where $r_>$ ($r_<$) is the length of the greater (smaller) of the two vectors $\mathbf{r}$ and $\mathbf{r}'$, we find

$$I=\sum_l \frac{4\pi}{2l+1}\sum_{L_i}\int dr\,r^2 R^*_{1L_1}(r)R_{3L_3}(r)\int dr'r'^2 \times R^*_{2L_2}(r')R_{4L_4}(r')\frac{r_<^l}{r_>^{l+1}}\sum_{m=-l}^{l} C_{L_3L_1L}C_{L_2L_4L}. \quad (38)$$

The coefficients $C_{LL'L''}$ are called Gaunt coefficients [see Eq. (A3) in the appendix]. If we define

$$C_{l;L_1L_2L_3L_4}\equiv\sum_{m=-l}^{l} C_{L_3L_1L}C_{L_2L_4L} \quad (39)$$

and

$$I_{l;L_1L_2L_3L_4}\equiv\int dr\,r^2 R^*_{1L_1}(r)R_{3L_3}(r) \times\int dr'r'^2 R^*_{2L_2}(r')R_{4L_4}(r')\frac{r_<^l}{r_>^{l+1}}, \quad (40)$$

the integral takes the form

$$I=\sum_{l,L_i}\frac{4\pi}{2l+1}C_{l;L_1L_2L_3L_4}I_{l;L_1L_2L_3L_4}. \quad (41)$$

The task is now to determine $I_{l;L_i}$ (we use the shorthand notation L_i for $L_1L_2L_3L_4$). To do this, we will use the formalism developed in the preceding section. In complete analogy to Eqs. (24)–(26) we now find

$$I_{l;L_i}=\sum_{p_i} a_{L_ip_i}b_{l;l_ip_i}, \quad (42)$$

where

$$a_{L_ip_i}=\prod_{i=1}^{2}[\delta_{p_i,0}A^*_{iL_i}+\delta_{p_i,1}B^*_{iL_i}]\prod_{i=3}^{4}[\delta_{p_i,0}A_{iL_i}+\delta_{p_i,1}B_{iL_i}] \quad (43)$$

and

$$b_{l;l_ip_i}=\int dr\,r^2[\delta_{p_1,0}\phi_{l_1}(r)+\delta_{p_1,1}\dot{\phi}_{l_1}(r)][\delta_{p_3,0}\phi_{l_3}(r) +\delta_{p_3,1}\dot{\phi}_{l_3}(r)]\int dr'\,r'^2[\delta_{p_2,0}\phi_{l_2}(r') +\delta_{p_2,1}\dot{\phi}_{l_2}(r')][\delta_{p_4,0}\phi_{l_4}(r')+\delta_{p_4,1}\dot{\phi}_{l_4}(r')]\frac{r_<^l}{r_>^{l+1}}. \quad (44)$$

It should be noted that these basic integrals are symmetric with respect to some of their indices. If we introduce the joined index $n_i=\{l_i,p_i\}$ then

$$b_{l;n_1n_2n_3n_4}=b_{l;n_3n_2n_1n_4}=b_{l;n_1n_4n_3n_2}=b_{l;n_3n_4n_1n_2}=b_{l;n_2n_1n_4n_3} =b_{l;n_2n_3n_4n_1}=b_{l;n_4n_1n_2n_3}=b_{l;n_4n_3n_2n_1}. \quad (45)$$

If we consider the numerical aspects for the case where *s*, *p*, *d*, and *f* orbitals are included in the wave-function expansion, we find that we need to use a cutoff of $l_{\max}=6$ in Eqs. (37) and (39). Using the symmetries in Eq. (45), we then find 9072 basic integrals that have to be calculated and stored. The sum in Eq. (41), however, involves $7\times16^4=458\,752$ elements. Fortunately, only 6778 combinations of the l, L_1, L_2, L_3, L_4 coefficients in Eq. (42) have to be calculated; the others vanish. Each of these coefficients involves a sum over 16 elements, and each of these elements is a product of five numbers.

2. Fast fourier transformation approach

The method we have just described works well, but requires a lot of Gaunt functions and other complications. As

mentioned, it also only involves integrals over the central site and ignores parts of the Wannier functions on nearby neighbors. We have therefore found a different approach to the problem.

To calculate $W(12,34;\mathbf{R},\mathbf{R}')$ for any lattice sites $\mathbf{R}$ and $\mathbf{R}'$, we make use of the Fourier transform

$$\int d^3\mathbf{q}\frac{e^{i\mathbf{q}\cdot\mathbf{r}}}{\mathbf{q}^2}=\frac{2\pi^2}{|\mathbf{r}|} \tag{46}$$

and find for Eq. (33)

$$W(12,34;\mathbf{R},\mathbf{R}')=\frac{e^2}{2\pi^2}\int\frac{d^3\mathbf{q}}{\mathbf{q}^2}e^{i\mathbf{q}\cdot(\mathbf{R}-\mathbf{R}')}f_{13}(\mathbf{q})f_{24}(-\mathbf{q}),$$

$$f_{ij}(\mathbf{q})\equiv\int d^3\mathbf{r}\,e^{i\mathbf{q}\cdot\mathbf{r}}w^*_{n_i}(\mathbf{R}-\mathbf{R}_i;\mathbf{r})w_{n_j}(\mathbf{R}-\mathbf{R}_j;\mathbf{r}). \tag{47}$$

The f_{ij} functions are just the Fourier transforms of a product of some Wannier functions in a sphere. These can be calculated very efficiently by calculating the Wannier functions on a cubic mesh in real space and then applying a standard FFT algorithm. To do this, we have used the routine ''fourn'' (cf. Ref. 33). For details on how to apply the FFT to continuous functions, Ref. 34 is very useful. The result of the Fourier transform is $f_{ij}(\mathbf{q})$ on a cubic mesh in $\mathbf{q}$ space with some Δq (the distance between the mesh points). We perform the remaining $\mathbf{q}$ integral in the following way. Let us call the integrand without the q^{-2} term

$$F(\mathbf{q})=e^{i\mathbf{q}\cdot(\mathbf{R}-\mathbf{R}')}f_{13}(\mathbf{q})f_{24}(-\mathbf{q}), \tag{48}$$

which is smooth function at $\mathbf{q}=\mathbf{0}$. In order to treat the divergence arising from q^{-2}, we split the integral in the following way:

$$\int d^3\mathbf{q}\frac{F(\mathbf{q})}{q^2}=\int d^3\mathbf{q}\frac{F(\mathbf{q})-F(\mathbf{0})}{q^2}+F(\mathbf{0})\int\frac{d^3\mathbf{q}}{q^2}. \tag{49}$$

All integrals are over a cube with length $N\Delta q$. The last integral is just half of this length times C, which we define as

$$C\equiv\int_{-1}^{+1}dx\int_{-1}^{+1}dy\int_{-1}^{+1}dz\frac{1}{r^2}\approx 15.348\,25. \tag{50}$$

The remaining integral in Eq. (49) is transformed into a sum over little cubes with volume $(\Delta q)^3$. For $\mathbf{q}=\mathbf{0}$ the value of the integrand is calculated via the second derivative of $F(\mathbf{q})$ at $\mathbf{q}=\mathbf{0}$ numerically (the second derivative is needed to cancel the q^2 in a power-law expansion of F).

The cubic grid in real space that we used to calculate the Wannier functions in Eq. (47) had $N=64^3$ points in the real space grid with a spacing $\Delta x=0.17$. The Δq spacing of the q mesh is determined by N and Δx. Using the FFT for continuous Fourier transformations one has to be very careful about the choice of these values because the FFT is a discrete Fourier transform. It is important to make sure that the results of a FFT calculation do not depend on the values N and Δx.

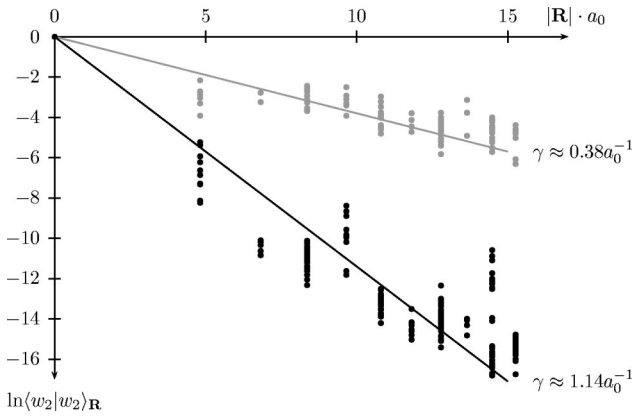

FIG. 1. Localization of Wannier functions before (gray) and after (solid) minimization of the spread functional Ω. Each dot represents the portion of the wave function in a muffin-tin sphere. The best exponential fit to the decay is roughly $e^{-\gamma r}$ with the values of γ given within the figure. In Eq. (10) we set $\mathbf{r}_0=(0.8,1.0,0.3)a_0$.

Note that each integral in Eq. (47) could be calculated from the spherical-harmonic expansions. However, many such integrals would be required and the method would be extremely computationally expensive. The FFT method generates all the $\mathbf{q}$ values needed with a single calculation and is much more efficient. However, because of finite mesh sizes and compromises between real and q space integrals, it is not as accurate as the spherical-harmonic expansion method of Sec. II E 1, when the latter is applicable.

III. RESULTS AND DISCUSSION

We have tested our methods on Cu, which has the following properties: (i) It has a simple close-packed fcc crystal structure for which the ASA should be a reasonable approximation. (ii) Cu is a simple metal that belongs to the $3d$ transition metals, so one can determine Coulomb matrix elements for the $3d$ states, which are interesting and of relevance for the really correlated $3d$ systems. (iii) Since Cu is nonmagnetic, we do not have to worry about spin-polarized or magnetic calculations. We have used the experimental lattice constant $a=3.614$ Å as given in Ref. 35. As usual we use atomic Rydberg units and $a_0=\hbar^2/me^2$ is the Bohr radius.

From the one-electron Bloch wave functions, the Wannier functions were obtained using 500 $\mathbf{k}$ points in the BZ. Since we have used a cutoff of $l_{\max}=3$, the LMTO method generates 16 bands. In the minimization procedure, all 16 bands were treated as a composite set of bands. To demonstrate the localization of the Wannier functions obtained, we have calculated

$$\langle w_n|w_n\rangle_{\mathbf{R}}=\int d^3r|w_n(\mathbf{R};\mathbf{r})|^2, \tag{51}$$

which is the relative weight the Wannier function localized at the site $\mathbf{0}$ has in the muffin-tin sphere centered around $\mathbf{R}$. In Fig. 1 we have plotted for $n=2$ the function $\ln\langle w_2|w_2\rangle_{\mathbf{R}}$ as a function of $|\mathbf{R}|$. Although the contribution to w_2 appears to

TABLE I. Angular character of Wannier functions in the center muffin-tin sphere (top) and first shell, i.e., 12 nearest neighbors (bottom).

l	$n=0$	1	2	3	4	5	6
(4)s	0.102	0.013	0.000	0.008	0.026	0.134	0.187
(4)p	0.297	0.131	0.058	0.042	0.151	0.373	0.392
(3)d	0.407	0.663	0.895	0.886	0.716	0.323	0.256
(4)f	0.096	0.140	0.024	0.039	0.064	0.069	0.051
Σ	0.902	0.947	0.977	0.975	0.956	0.899	0.886
(4)s	0.009	0.004	0.002	0.002	0.004	0.009	0.011
(4)p	0.019	0.008	0.004	0.004	0.008	0.020	0.023
(3)d	0.052	0.029	0.012	0.013	0.024	0.053	0.060
(4)f	0.012	0.008	0.003	0.003	0.006	0.012	0.013
Σ	0.092	0.049	0.021	0.023	0.041	0.094	0.107

decrease exponentially with increasing distance from the central sphere when plotted in this way, i.e., our Wannier functions are exponentially localized, we actually get just as good a fit through the scatter of the data with a power-law dependence with a power of about -7. It is not easy to numerically decide whether the decay is an exponential or a power-law dependence, since our Wannier functions are ultimately periodic in a supercell determined by the $\Delta\mathbf{k}$ spacing of the discrete $\mathbf{k}$ mesh used to construct them. In either case, the Wannier function is highly localized. The gray dots and line in the figure show the result when only the phase has been adjusted according to Eq. (10); then the Wannier functions have a relatively smaller decay constant of $\gamma = 0.38 a_0^{-1}$. The black dots and line show the result after the full localization (minimization) procedure of Ref. 27 has been applied by minimizing the full set of all 16 bands considered; clearly a much better localization with a larger decay constant $\gamma = 1.14 a_0^{-1}$ has been achieved. When we tried to minimize a smaller subset of bands (five bands instead of the full 16) the decay factor was in between the other two values, with $\gamma \approx 0.71 a_0^{-1}$ (not shown in the figure).

Here we should note that the Wannier functions are not pure in terms of their l character. Table I shows the angular character in the center muffin tin (MT) and the first shell for the first seven Wannier states. We see that for the states with $n=0$ to $n=4$ the d character is largest, which suggests to call these states d-like states yielding five d states per spin direction as expected. But among these states the d character is highest (nearly 90%) for the states $n=2$ and 3. Table I also tells us how much of the state is found in the center muffin tin. We see that the state $n=2$ has 97.7% in the center MT and only 2.1% in the next shell demonstrating how well localized this Wannier function is. The Wannier functions corresponding to $n=0$, $n=5$, and $n=6$ have considerable $4s$ and $4p$ character, and $n=5$ and $n=6$ have the least $3d$ character. But they are very well localized as well, having at least 88% of their total weight already within the central muffin-tin sphere. On the other hand, all Wannier states are mixed with respect to their l character, since the minimization procedure mixes all the l characters.

Figure 2 shows a few radial-averaged Wannier functions

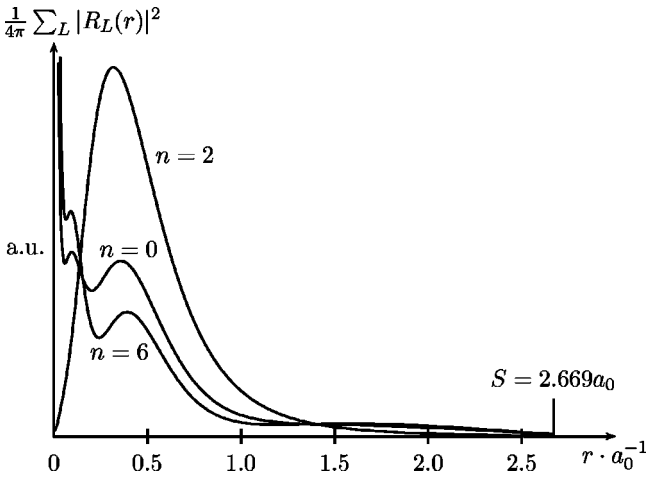

FIG. 2. Radial-averaged Wannier functions in the center muffin-tin sphere for various indices n.

in their center MT. We should note that the peak of the states $n=0$ and 6 for $r \to 0$ does not contribute very much to matrix elements because of the r^2 in Eq. (22). Figure 2 may also be qualitatively compared with the Wannier function of Cu in Ref. 36.

From these Wannier functions we have calculated the hopping matrix elements $t_{\mathbf{R}nm}$ according to Eq. (19). These can be inserted into Eq. (18) in order to determine an effective orthogonalized (diagonal S-matrix) tight-binding representation. The matrices $H^{\mathbf{k}}$ are not diagonal because the unitary matrix that was used in the minimization of the Wannier functions scrambled the different bands. However, we can still diagonalize $H^{\mathbf{k}}$ for each k point and compare the eigenvalues with the original LDA band structure. The results are shown in Fig. 3, where we have cutoff the $\mathbf{R}$ sum in Eq. (18) to include only $\mathbf{0}$ and the 3 nearest shells, i.e., 43 sites. We have found that the decay of $t_{\mathbf{R}nm}$ as a function of $|\mathbf{R}|$ is a lot faster than that of the Fourier components of the band structure, Eq. (17). If we just take Eq. (17) and recalculate the band structure according to Eq. (18), the agreement is a lot worse (for the same number of sites in $t_{\mathbf{R}nn}$). This can be understood in the following way: Labeling the bands accord-

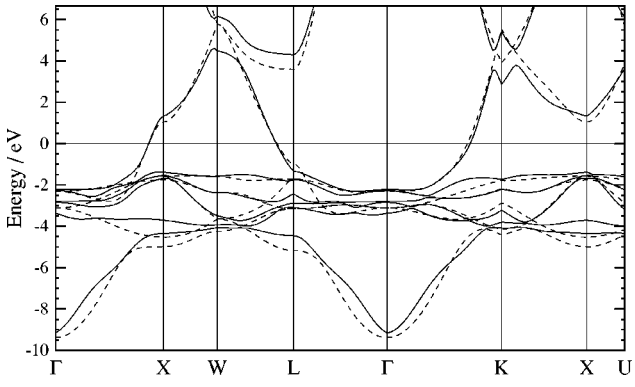

FIG. 3. Comparison of LDA band structure (dashed line) and the diagonalized eigenvalues of Eq. (18), where three shells in the lattice sum were included. The bands are relative to the Fermi level at 0 eV.

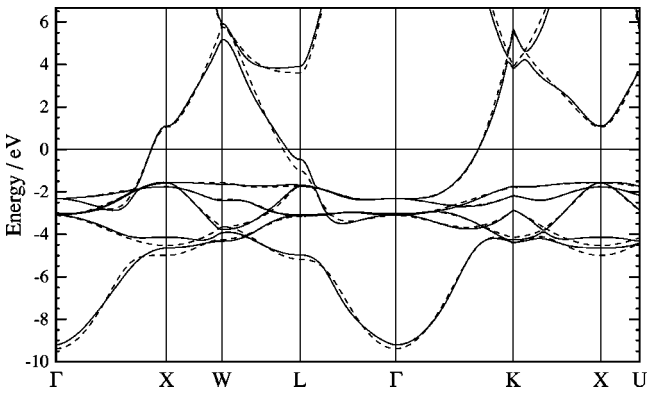

FIG. 4. Comparison of LDA band structure (dashed line) and the diagonalized eigenvalues of Eq. (18), where eight shells in the lattice sum were included.

ing to $E_n(\mathbf{k}) < E_{n+1}(\mathbf{k})$ is not "natural," therefore at points in k space where two bands cross each other $E_n(\mathbf{k})$ has a kink. Those kinks have non-negligible Fourier components with large $|\mathbf{R}|$, which our cutoff sets to zero.

In Fig. 4 we have included eight shells in the lattice sum of Eq. (18), i.e., 141 sites. As we can see the two curves agree even better. These calculations are a test of the quality of the Wannier functions, i.e., how well the matrix elements obtained from these Wannier functions reproduce the known band structure.

With respect to the magnitude of the hopping matrix elements, the $t_{\mathbf{0}nm}$ are largest and provide information about the positions of the bands. For a next neighbor $\mathbf{R}$, the $|t_{\mathbf{R}nm}|$ are of the order of 0.3 eV for d states (and 1 eV for the state with $n=0$). For larger $\mathbf{R}$ the hopping matrix elements are less than 0.15 eV for d states (and less than 0.5 eV for the state with $n=0$).

Next, consider the projected DOS. In these calculations we have used the tetrahedron method[31] (see also Ref. 23) with 200 $\mathbf{k}$ points and 691 tetrahedron in the irreducible part of the Brillouin zone. In Fig. 5 we have plotted the total DOS, which can also be found in the literature (see Ref. 37).

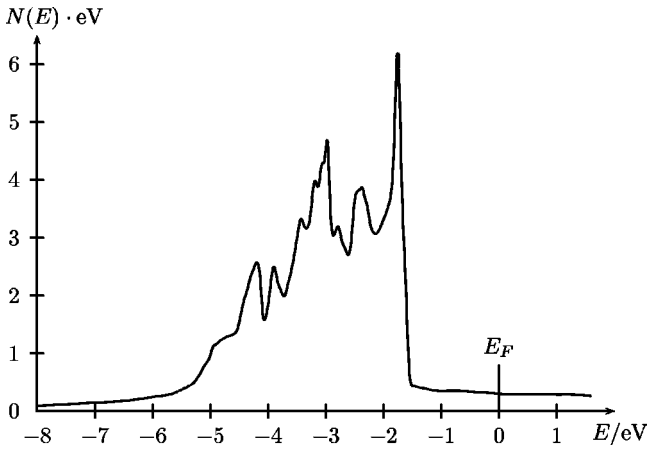

FIG. 5. Total electronic density of states, relative to the Fermi energy. We have used a Gaussian broadening of 2 mRy to remove the spikes inherent in the linear tetrahedron method.

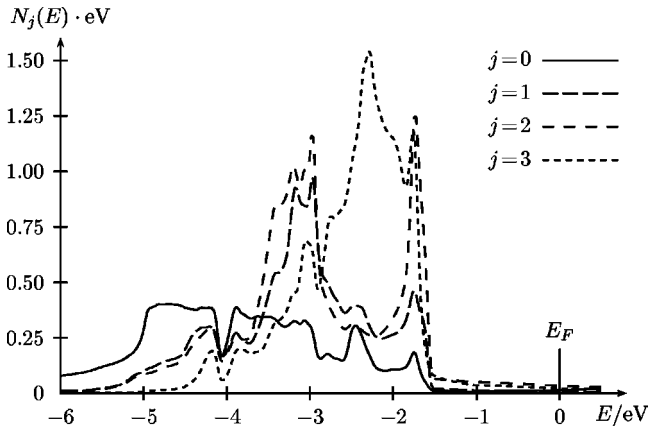

FIG. 6. Projected DOS for Wannier states 0–3.

Figures 6 and 7 show the projected DOS according to Eq. (28) for the Wannier functions 0–7. It is interesting that states $j=2$ and 3 have very similar l character (cf. Table I) but a very different projected DOS in Fig. 6, i.e., they are peaked at different energies and emphasize different parts of the d band. Table II shows the projected density of states (actually the percentage of the DOS in different states) and the projected number of states evaluated at the Fermi level, where the jth projected number of states is defined as

$$n_j(E_F) = \int^{E_F} dE\, N_j(E). \tag{52}$$

This is just the number of electrons in the jth state. Every state could maximally be occupied with two electrons (one for each spin direction).

We next consider a calculation of the direct Coulomb integral U_{ii} for a d-like orbital with itself. As discussed above, the Wannier function for $n=2$ has nearly perfect d character and to a good approximation we can consider only its contribution in the central MT, i.e., at site $\mathbf{0}$. What we then calculate is the on-site Coulomb matrix element between two electrons (with different spin because of the Pauli principle) at the same site in the same Wannier state, i.e., essentially the Hubbard U in its original sense.[3] The method described in Sec. II E 1 yields $U(dd;\mathbf{0},\mathbf{0}) = 25.26$ eV while the method from Sec. II E 2 yields 25.16 eV for this quantity. But with the second method we are able to calculate all the elements involving tails of the Wannier functions in other muffin tins in the double sum in Eq. (32). When we do this and include

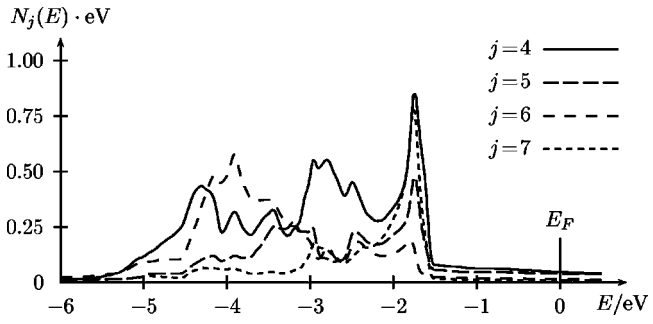

FIG. 7. Projected DOS for Wannier states 4–7.

TABLE II. Projected number of states at the Fermi energy, i.e., $n_j(E_F)$. For $j>8$ (the numbers not given), $n_j(E_F)<0.25$. The second line shows the percentage of the DOS at Fermi energy, i.e., $100N_j(E_F)/N(E_F)$.

j	0	1	2	3	4	5	6	7	8
$n_j(E_F)$	1.17	1.31	1.59	1.80	1.34	0.66	0.90	0.51	0.78
% DOS	4.7	2.1	11.1	7.1	15.4	13.0	4.6	3.2	27.3

sites where $\mathbf{R}_i$ and $\mathbf{R}_j$ are nearest neighbors, we get $U_{dd}=25.51$ eV, which shows that including the portions of the Wannier function on neighboring sites is a rather small correction on U for such a strongly localized function. Table III show these quantities for the Wannier functions $n=0$ through 6. Going beyond nearest neighbors would have even a smaller effect. Therefore, one can truncate the sums over higher neighbor shells for the Coulomb matrix elements, which converge faster than for the hopping matrix elements. The reason for this is that the Coulomb integral involves a product of four wave functions, whereas the hopping matrix elements involve only two wave functions.

The FFT approach allows us to calculate Coulomb matrix elements for Wannier functions centered on different sites. We have done this for the states $a=\{\mathbf{0},2\}$ and $b=\{\mathbf{R},2\}$ where $\mathbf{R}$ is a nearest neighbor of $\mathbf{0}$. Both are d-like states. In Eq. (32) we have again included nearest neighbors for $\mathbf{R}_i$ and $\mathbf{R}_j$. The result is $U_{ab}=5.87$ eV. The largest contribution in the sum is $U(ab;\mathbf{0},\mathbf{R})=5.66$ eV, which is the contribution arising from the two center spheres of states a and b.

Our first method is most useful for calculating interband (on-site) Coulomb matrix elements when the states are so well localized that we can neglect the contribution from neighboring spheres. We have calculated both the direct Coulomb matrix elements U_{nm} and the exchange integrals J_{nm} for all n and m. Here the n,m just indicates the band and all Wannier states are centered at site $\mathbf{0}$. The results are given in Tables IV and V for the first seven bands. We see that the on-site intraband Coulomb matrix elements are largest for the Wannier states $n=2$ and 3, which have almost pure d character. We also note that all the direct Coulomb matrix elements U_{nm} are rather large, while the exchange Coulomb matrix elements J_{nm} with $n\neq m$ are rather small [note that the diagonal terms for both U_{ii} and J_{ii} are identical by definition, cf. Eq. (34)]. When we compare the diagonal elements U_{nn} $(=J_{nn})$ from Tables IV and V with the first line of Table III we note relatively large differences for the states $n=0$, 5, and 6, which have large s and p character, as can be

TABLE III. On-site FFT U's. In the first line (on-site U) we have only included $\mathbf{R}_i=\mathbf{R}_i=\mathbf{0}$ in Eq. (32), i.e., $U(jj;\mathbf{0},\mathbf{0})$. The second line (NN U) shows the same quantity, where we have included nearest neighbors for $\mathbf{R}_i$ and $\mathbf{R}_j$.

j	0	1	2	3	4	5	6
on-site-U	14.82	19.05	25.16	25.49	20.79	13.81	13.22
NN-U	16.29	19.81	25.51	25.86	21.44	15.32	14.97

TABLE IV. Interband on-site matrix elements, U_{nm} in eV.

	$m=0$	1	2	3	4	5	6
$n=0$	14.30	15.86	17.86	17.45	16.31	13.24	12.77
1	15.86	19.02	21.36	20.98	19.33	15.25	14.42
2	17.86	21.36	25.26	24.13	22.30	17.09	15.86
3	17.45	20.98	24.13	25.26	21.88	16.69	16.12
4	16.31	19.33	22.30	21.88	20.70	15.76	14.78
5	13.24	15.25	17.09	16.69	15.76	13.23	12.32
6	12.77	14.42	15.86	16.12	14.78	12.32	12.43

seen from Table I (e.g., 0.52 eV for $n=0$). This leads to a peak in their charge density near $\mathbf{r}=\mathbf{0}$ as we can see from Fig. 2 for $n=0$ and 6. For those states our FFT calculations had a numerical problem because our real-space grid was too large (with $\Delta x=0.17a_0$). But for $n=2$, we do not have a peak at $\mathbf{r}=\mathbf{0}$, and the FFT approach does an excellent job.

The Hubbard U clearly depends on the specific shape of the Wannier functions. Intuitively, one expects bigger U's for more localized orbitals. As an example of this, we have calculated a less-localized Wannier state (by performing fewer steps in the minimization procedure). In this case, the highest d-character state, which is almost pure d like, has only 58.5% of its charge density in the center muffin tin, and 95.4% within the first three shells. For those three shells we have used the FFT method to calculate all 43^2 terms (33). We find $U=13.8$ eV for this less-localized d state.

We should also note that most model calculations assume very localized, pure (in l character) Wannier functions. In particular, they often assume that LDA or some one-electron-like treatment is adequate for non-d and non-f electron states, and that the only explicit correlations that need to be included are related to on-site (or sometimes also nearest-neighbor) Coulomb U's for the d (or f) states. It is also often implicitly assumed that the non-d and non-f states have some screening contribution to the effective U's in the model Hamiltonian. These types of assumptions raise some difficulties for us to connect our treatment to the model Hamiltonians, since the orthogonalization properties and mixing necessary for localizing our Wannier functions scramble the l character of the resulting orbitals. Hence, our effective U's do not have a pure d or f character (or s or p). Also, since we calculate U's for all of the orbitals, we are implicitly including correlation effects for all orbital (s and p as well as d and f), and however the U's in our treatment are ultimately

TABLE V. Interband on-site matrix elements, J_{nm} in eV.

	$m=0$	1	2	3	4	5	6
$n=0$	14.30	0.91	0.73	0.76	0.92	0.98	1.34
1	0.91	19.02	1.22	0.84	0.91	1.43	0.69
2	0.73	1.22	25.26	0.92	1.14	0.95	0.58
3	0.76	0.84	0.92	25.26	0.99	0.71	0.62
4	0.92	0.91	1.14	0.99	20.70	1.20	0.79
5	0.98	1.43	0.95	0.71	1.20	13.23	1.22
6	1.34	0.69	0.58	0.62	0.79	1.22	12.43

screened in some many-body treatment, this screening may be different from that assumed in the model Hamiltonians. We may ultimately be forced to use some kind of projection of our orbitals onto pure l-character states in order to make appropriate identification between our types of states and more conventional model Hamiltonians.

IV. CONSTRAINED LDA

Finally, we have done a constrained LDA calculation[17] to obtain an estimate for the Hubbard U. In this method the Hubbard U is defined as the Coulomb energy cost to place two (in our case d) electrons at the same site. This is

$$U=E(N_d+1)+E(N_d-1)-2E(N_d). \tag{53}$$

Here $E(N_d)$ is the ground-state energy with N_d d electrons. If we consider this energy as a continuous function of N_d, where we constrain the value of N_d to be away from its minimized value, then the Hubbard U is given by

$$U_{dd}=\frac{\delta^2 E(N_d)}{\delta N_d^2}. \tag{54}$$

This constraint, which fixes the total number of d electrons to be N_d, can be taken into account by adding a Lagrange parameter v_d to the total energy; i.e., the energy of the constrained system is given by

$$E(N_d)=\min\left[E\{n(\mathbf{r})\}+v_d\left\{\int d^3r n_d(\mathbf{r})-N_d\right\}\right]. \tag{55}$$

Here $E\{n(\mathbf{r})\}$ is the usual band-structure energy and $n_d(\mathbf{r})$ is the d-electron density. On minimization, the extra term in Eq. (55) leads to an additional constant potential v_d in the Kohn-Sham equations, which acts only on the $l=2$ angular momentum components of the wave function. Within the LMTO method, this is accomplished by adding a constant potential v_d when solving the radial Schrödinger equation for $l=2$, and then calculating the total energy as a function of v_d. Since each value of v_d changes the d occupation number, the final result can be written as $E(N_d)$. This dependence is shown in Fig. 8 and can be accurately fitted by a parabola $\delta E=\frac{1}{2}U_{dd}N_d^2$ with $U_{dd}=18.2$ eV. This is of the same magnitude as the result obtained from the direct calculation of the Coulomb matrix elements, even though one might expect a smaller value because of the screening effects that are believed to be included in this calculation. In our calculations we have only used a one-atom unit cell. If a larger unit cell is chosen, one could do a variety of additional constraints (e.g., changing the d occupation separately on two different atoms). Such calculations could attempt to sort out more details of effective Hamiltonians (perhaps even two-particle parameters). However, such calculations would take our work in a different direction from the one we are interested in. Also, given the intuitive nature of the constrained method and the difficulties in fitting such a large parameter space, it is not clear how useful the resulting parameters would be or their uniqueness.

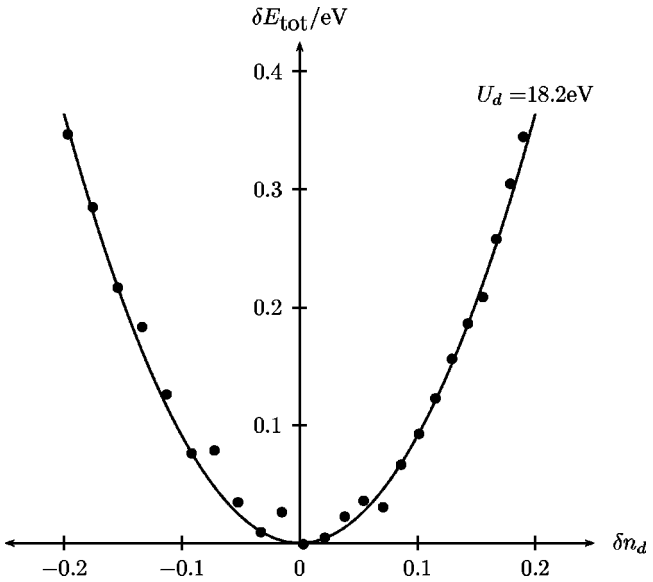

FIG. 8. The total energy as a function of the effective change in d charge. The line is a quadratic fit.

V. CONCLUSIONS

We have shown in this paper that *ab initio* band-structure methods can be used for a first-principles calculation of well-localized Wannier functions, which is achieved by using a method proposed by Marzari and Vanderbilt.[27] From these localized Wannier functions the on-site and intersite one-particle matrix elements of the Hamiltonian can be calculated. A good localization of the Wannier functions is needed to keep tight-binding (hopping) matrix elements restricted to a small number of near neighbors. The Coulomb matrix elements within these localized Wannier states can also be calculated and are similarly only important between on-site and nearest-neighbor Wannier functions. The result is thus an electronic multiband Hamiltonian in second quantization with first-principles one- and two-particle matrix elements. The Hamiltonian is of the form of an extended multiband Hubbard model but without adjustable parameters; the parameters are directly calculated for a given material. The only approximations still involved are the ones inherent to the *ab initio* band-structure method used (e.g., the muffin-tin assumption, the ASA approximation, the choice of linearized orbitals in the LMTO, and the ''frozen-core'' approximation), and the truncation in the number of bands (states) per site that is explicitly taken into account (truncation of the l sum). The resulting multiband Hamiltonian that includes the Hubbard-U terms, of course, still has to be studied within a reliable many-body method or approximation, e.g, a multiband version of the DMFT as in Refs. 7, 10, 12, and 14.

Our Cu calculations yield on-site direct Coulomb matrix elements (''Hubbard U's'') of the magnitude of 20 eV for 3d Wannier states and inter-site (Hubbard U's between nearest neighbors) values of 5 eV. This is the magnitude discussed already earlier[3] and similar to those for atomic 3d states. These U values are much larger than commonly expected or used in model studies. Although our calculated Coulomb matrix elements are unscreened, the constrained LDA, which

includes some screening effects, gives comparable magnitudes for U. Since dynamic screening due to the mobile electrons in the outer shells (bands) is taken into account automatically when using an appropriate many-body method, e.g., a generalized random-phase approximation, the only screening that should be included in a better theory is a static, short-range screening by the inner core electrons. However, the (atomic-like) electronic states representing the inner (''frozen'') core are well known, and it should be possible to calculate their screening contribution from a (generalized) static Lindhard theory. In future work we plan to examine the static screening due to the inner core states, an application of appropriate (multiband) many-body methods, and the application to more strongly correlated 3d materials such as iron, cobalt, and nickel. Any treatment of screening will, of course, have to be done very carefully so that screening effects are not double counted (once in the explicit screening and then a second time when the many-body Hamiltonian is solved). Finally, although any localized orbitals could be used as the basis for a many-body treatment, the approach we have used (of constructing localized orbitals from LDA band states) has the advantage that these orbitals are a good basis set for any states without strong electron-electron correlations, since LDA is believed to be an accurate approximation in this limit. We can hope that an additional more explicit treatment of the strong correlations by a many-body theory will correct and improve on the LDA starting point.

ACKNOWLEDGMENTS

This research was partially supported by the Department of Energy under contract W-7405-ENG-36. This research used resources of the National Energy Research Scientific Computing Center, which is supported by the Office of Science of the U.S. Department of Energy under Contract No. DE-AC03-76SF00098. We also acknowledge a generous grant from the University of Bremen for a visit by one of us (R.C.A.) that helped make possible this work. We thank Veljko Zlatic for suggesting the application of the FFT algorithm in the Coulomb matrix-element calculations.

APPENDIX: SPHERICAL HARMONICS EXPANSIONS

Any function $A(\mathbf{r})$ within a (muffin-tin) sphere may be expanded in terms of spherical harmonics,

$$A(\mathbf{r})=\sum_L A_L(r)Y_L(\hat{\mathbf{r}}) \tag{A1}$$

If two functions $A(\mathbf{r})$ and $B(\mathbf{r})$ are given via their coefficients $A_L(r)$ and $B_L(r)$, then the corresponding coefficients $F_L(r)$ of the function $F(\mathbf{r})=A(\mathbf{r})B(\mathbf{r})$ are given by

$$F_L(r)=\sum_{L_1,L_2} A_{L_1}(r)B_{L_2}(r)C_{L_1LL_2}. \tag{A2}$$

The Gaunt coefficients $C_{LL'L''}$ are defined by

$$C_{LL'L''}=\int d^2\Omega\, Y_L(\Omega)Y^*_{L'}(\Omega)Y_{L''}(\Omega)$$

$$=\delta_{m'',m'-m}\sqrt{\frac{2l''+1}{4\pi}}c^{l''}(L',L) \tag{A3}$$

and the $c^k(L',L)$ are tabulated in Ref. 38. We may use Eq. (A2) to multiply a function with a plane wave $e^{\mathbf{k}}(\mathbf{r})\equiv e^{-i\mathbf{k}\cdot\mathbf{r}}$ whose coefficients are given by (see Ref. 32)

$$e^{\mathbf{k}}_L(r)=4\pi j_l(kr)[i^l Y_L(\hat{\mathbf{k}})]^*. \tag{A4}$$

[1] P. Hohenberg and W. Kohn, Phys. Rev. **136**, B864 (1964).
[2] W. Kohn and L.J. Sham, Phys. Rev. **140**, A1133 (1965).
[3] J. Hubbard, Proc. R. Soc. London, Ser. A **276**, 238 (1963).
[4] V.I. Anisimov, J. Zaanen, and O.K. Andersen, Phys. Rev. B **44**, 943 (1991).
[5] M.M. Steiner, R.C. Albers, D.J. Scalapino, and L.J. Sham, Phys. Rev. B **43**, 1637 (1991).
[6] M.M. Steiner, R.C. Albers, and L.J. Sham, Phys. Rev. B **45**, 13 272 (1992); Phys. Rev. Lett. **72**, 2923 (1994).
[7] V.I. Anisimov, A.I. Poteryaev, M.A. Korotin, A.O. Anokhin, and G. Kotliar, J. Phys.: Condens. Matter **9**, 7359 (1997).
[8] A.I. Lichtenstein and M.I. Katsnelson, Phys. Rev. B **57**, 6884 (1998).
[9] V. Drchal V. Janis, and J. Kudrnovsky, Phys. Rev. B **60**, 15 664 (1999).
[10] M.I. Katsnelson and A.I. Lichtenstein, J. Phys.: Condens. Matter **11**, 1037 (1999).
[11] A. Liebsch and A.I. Lichtenstein, Phys. Rev. Lett. **84**, 1591 (2000).
[12] M.B. Zölfl, T. Pruschke, J. Keller, A.I. Poteryaev, I.A. Nekrasov, and V.I. Anisimov, Phys. Rev. B **61**, 12 810 (2000).
[13] T. Wegner, M. Potthoff, and W. Nolting, Phys. Rev. B **61**, 1386 (2000).
[14] I.A. Nekrasov, K. Held, N. Blümer, A.I. Poteryaev, V.I. Anisimov, and D. Vollhardt, Eur. Phys. J. B **18**, 55 (2000).
[15] For a review see: A. George, G. Kotliar, W. Krauth, and M.J. Rozenberg, Rev. Mod. Phys. **68**, 13 (1996).
[16] W. Metzner and D. Vollhardt, Phys. Rev. Lett. **62**, 324 (1989).
[17] P.H. Dederichs, S. Blügel, R. Zeller, and H. Akai, Phys. Rev. Lett. **53**, 2512 (1984).
[18] Mark S. Hybertsen, M. Schlüter, and Niels E. Christensen, Phys. Rev. B **39**, 9028 (1988).
[19] A.K. McMahan, R.M. Martin, and S. Satpathy, Phys. Rev. B **38**, 6650 (1988).
[20] O. Gunnarsson, O.K. Andersen, O. Jepsen, and J. Zaanen, Phys. Rev. B **39**, 1708 (1989).
[21] A.K. McMahan, J.F. Annett, and R.M. Martin, Phys. Rev. B **42**, 6268 (1990).
[22] M. Alouani, R.C. Albers, and J.M. Wills, Synth. Met. **55-57**, 3358 (1993).

[23] H. L. Skriver, *The LMTO Method* (Springer-Verlag, Berlin, 1984).
[24] O.K. Andersen, Phys. Rev. B **12**, 3060 (1975).
[25] G.H. Wannier, Phys. Rev. **52**, 191 (1937).
[26] J. Callaway, *Quantum Theory of the Solid State* (Academic, San Diego, 1974).
[27] N. Marzari and D. Vanderbilt, Phys. Rev. B **56**, 12 847 (1997).
[28] A. Svane and O.K. Andersen, Phys. Rev. B **34**, 5512 (1986).
[29] R. M. Dreizler and E. K. U. Gross, *Density Functional Theory* (Springer, New York, 1990).
[30] U. von Barth and L. Hedin, J. Phys. C **5**, 1629 (1972).
[31] O. Jepsen and O.K. Andersen, Solid State Commun. **9**, 1763 (1971); G. Lehmen and M. Taut, Phys. Status Solidi B **54**, 469 (1972).
[32] J.D.Jackson, *Classical Electrodynamics* (John Wiley, New York, 1975).
[33] W. H. Press, S. A. Teukolsky, W. T. Vetterling, and B. P. Flannery, *Numerical Recipes in C* (Cambridge University Press, Cambridge, UK, 1992).
[34] E. Oran Brigham, *The Fast Fourier Transform* (Prentice-Hall, Englewood Cliffs, NJ, 1974).
[35] N. W. Ashcroft and N. D. Mermin, *Solid State Physics* (Saunders, Philadelphia, 1976).
[36] H. Eschrig, *Optimized LCAO Method* (Springer, New York, 1989).
[37] V. L. Moruzzi, J. F. Janak, and A. R. Williams, *Calculated Electronic Properties of Metals* (Pergamon, New York, 1978).
[38] E. U. Condon and G.H. Shortley, *The Theory of Atomic Spectra* (Cambridge University Press, Cambridge, England, 1953).